Geophysical Research Letters

RESEARCH LETTER
10.1029/2019GL083426

Time-Lag Correlation Between Passive Microwave Measurements and Surface Precipitation and Its Impact on Precipitation Retrieval Evaluation

Yalei You[1], Huan Meng[2], Jun Dong[1], and Scott Rudlosky[2]

[1]Earth System Science Interdisciplinary Center/Cooperative Institute for Climate and Satellites, University of Maryland, College Park, MD, USA, [2]National Oceanic and Atmospheric Administration/National Environmental Satellite, Data, and Information Service, College Park, Maryland, USA

Abstract This study investigates the correlation between the upwelling microwave brightness temperature measured by satellite radiometer and surface precipitation rate from ground radar observations at different time lags. Results show that brightness temperatures correlate more strongly with the lagged surface precipitation rate than the simultaneous surface precipitation rate. The lag time for snowfall ranges from 30 to 60 min. This time lag effect has an important influence when evaluating the satellite retrieval results relative to ground observations. For example, the falsely identified pixels can decrease by as much as 23.88% when considering a 30-min lag time. Furthermore, the satellite-retrieved snowfall rate shows much stronger correlation with the time-lagged surface snowfall rate than the simultaneous snowfall rate in cold environments and for tall storms. This work implies that the time of the level-2 swath-retrieved snowfall rate needs to shift forward when incorporated into the level-3 gridded products.

Key Points:
- The lag time between brightness temperature and the surface snowfall rate ranges from 30 to 60 min
- Weak correlation between satellite-retrieved snowfall rate and surface observations may not indicate poor retrieval performance
- A 30-min time lag is recommended when incorporating the level 2 swath snowfall rate into the level 3 gridded products

Correspondence to:
Y. You,
yyou@umd.edu

Citation:
You, Y., Meng, H., Dong, J., & Rudlosky, S. (2019). Time-lag correlation between passive microwave measurements and surface precipitation and its impact on precipitation retrieval evaluation. *Geophysical Research Letters*, *46*, 8415–8423. https://doi.org/10.1029/2019GL083426

Received 23 APR 2019
Accepted 2 JUL 2019
Accepted article online 9 JUL 2019
Published online 16 JUL 2019

1. Introduction

Level-2 (swath) precipitation estimates derived from passive microwave observations provide a major information source for the widely used level-3 (gridded) precipitation data sets (e.g., NASA's integrated multisatellite retrievals, IMERG, Huffman et al., 2015, and Climate Prediction Center's morphing technique, CMORPH, Xie et al., 2017). More than 10 spaceborne passive microwave radiometers are operational from several international agencies (Dong et al., 2009; Edwards & Pawlak, 2000; Hou et al., 2014). Brightness temperature (TB) observations from these passive microwave radiometers are combined with infrared sensor observations to produce global high-quality precipitation estimates every 30 min. Several planned satellite missions also will house radiometers suitable for precipitation estimation (Goldberg, 2018; Gu & Tong, 2015).

Many precipitation retrieval algorithms have been developed to estimate the precipitation rate from passive microwave TB observations (e.g., Aonashi et al., 2009; Boukabara et al., 2011; Ebtehaj et al., 2015; Ferraro & Marks, 1995; Kummerow et al., 2015; Kidd et al., 2016; You et al., 2015, 2016). These algorithms often produce more accurate rainfall estimates. It remains challenging to accurately estimate the snowfall rate by passive microwave radiometers, due to the large surface emissivity variation (Foster et al., 2012), the weak hydrometeor scattering signature (Munchak & Skofronick-Jackson, 2013; You et al., 2015), the complex radiative properties of snowflakes (Liu, 2008; Petty & Huang, 2010), and the possible contamination from supercooled liquid water (Kulie et al., 2010; Wang et al., 2013). A current international satellite constellation mission (Global Precipitation Measurement Mission), led by National Aeronautics and Space Administration (NASA) and the Japan Aerospace and Exploration Agency (JAXA), is designed to improve the global precipitation measurement accuracy (Skofronick-Jackson et al., 2017). Regardless of snowfall or rainfall, these retrievals are often assumed to be the instantaneous surface precipitation rate within the satellite footprint at the time of the satellite observation, even when incorporated into the level-3 gridded data sets.

However, TB is not directly proportional to the instantaneous surface precipitation rate. Rather, it encompasses the integrated effects from the hydrometeors in the entire precipitation column (e.g., Petersen & Rutledge, 2001; Wang et al., 2018; You & Liu, 2012). Furthermore, TB at different frequencies are sensitive to hydrometeors at different altitudes to varying degrees (Bennartz & Petty, 2001; Skofronick-Jackson

& Johnson, 2011; You et al., 2017). For example, under light and moderate precipitation scenarios, low-frequency TBs tend to be more sensitive to the hydrometeors at lower altitudes relative to the higher-frequency channels (e.g., 166 and 183.3 ± 7 GHz). These intrinsic TB attributes indicate that precipitation rates retrieved from TB are only an approximation of the surface precipitation rate at the time of the satellite observation. The accuracy of this approximation depends on how long it takes for the satellite-observed hydrometeors to reach the ground. The hydrometeor taking time to reach the ground is similar in concept to the ground soil taking time to respond to rainfall (Li & Min, 2013). Precipitation retrieval algorithms have been developed by either linking the hydrometeor amount in the air to the surface precipitation rate, or linking the surface soil moisture variation to the precipitation rate. Spaceborne sensors in this study are designed to measure the hydrometeor effect.

The time-lag correlation between rainfall rate estimated from spaceborne instruments and surface gauge observations was examined by Amitai et al. (2012) and Tan et al. (2018). Both studies concluded that the correlation between gauge-observed rain rate and the rain rate estimated from the spaceborne sensors peaks later in time (<20 min). They related this observation to the time it takes for the raindrops to reach the gauge from the time they are observed by the spaceborne sensors. Meng et al. (2017) also observed time lag in the satellite retrieved snowfall rate. They found that snowfall rates observed by the Advanced Technology Microwave Sounder (ATMS) correlated most strongly with the surface snowfall rate at a ~30-min lag.

As expected, this lag-time characteristics in level-2 swath data propagates into the level-3 merged data set. Villarini and Krajewski (2007) showed that the optimal performance for Tropical Rainfall Measuring Mission (TRMM) Multisatellite Precipitation Analysis (TMPA) data set was achieved by shifting the TMPA nominal time forward ~20 to 60 min, when comparing with the rain gauge observations in Oklahoma. Foelsche et al. (2017) concluded that the optimal lag time was ~40 min when comparing the GPM IMERG data set with rain gauge observations in southeastern Austria.

This study investigates the time lag between surface precipitation rate and TBs at different frequencies. This analysis helps explain why the satellite retrieved precipitation rate often correlates more strongly with surface instrument observations at a later time. This study then evaluates the effect of the time lag on the satellite precipitation detection and retrieval performance using the surface observations as the reference. Our analysis seeks to identify a suitable lag time for incorporating the level-2 swath precipitation rate into the level-3 gridded precipitation product.

2. Data

The primary data are Global Precipitation Measurement (GPM) Imager (GMI) TBs, Goddard Profiling Algorithm (GPROF) precipitation retrievals for GMI, and ground-based radar observations over the Contiguous United States (CONUS) from March 2014 to December 2017. The GMI TBs at 89.0 (V/H), 165.6 (V/H), 183.31±3 (V), and 183.31 ± 7 (V) GHz are used, with V and H representing the vertical and horizontal polarization, respectively. The mean footprint resolution is ~7 km for 89 GHz, and ~6 km for 165.6, 183.31 ± 3, and 183.31 ± 7 GHz (Draper et al., 2015). Hereafter, these frequencies are referred to as V89, H89, V166, H166, V186, and V190. The near surface precipitation rate retrieved by GPROF for GMI is at the 18.7-GHz footprint size resolution (~15 km, Kummerow et al., 2015).

The ground reference is the precipitation rate from the ground-based radar observations at 0.01° and 2-min spatial and temporal resolution (Multiradar/Multisensor System-MRMS; Zhang et al., 2016). Only MRMS data with the radar quality index greater than 0.8 are used. The time lag is analyzed separately for rain and snow. The precipitation phase definition uses both MRMS and the Ku-band precipitation radar (KuPR) onboard GPM satellite to account for uncertainty in the MRMS snowfall classification (see section 3c).

Although this study assumes the MRMS precipitation rate as the "surface precipitation rate," the MRMS derives the precipitation rate using the lowest radar scans that are not severely blocked by terrain. Terrain blockage can lead to MRMS-derived precipitation rates that actually measure precipitation well above the surface. To mitigate this issue, only data with the beam bottom height less than 500 m are selected. It is expected that use of gauge observations as the surface reference will lead to longer lag times than those identified herein.

The ancillary parameters include the storm top height from KuPR, and the hourly 2-m air temperature and 3-hourly temperature profile at 0.5° × 0.625° from Modern-Era Retrospective analysis for Research and

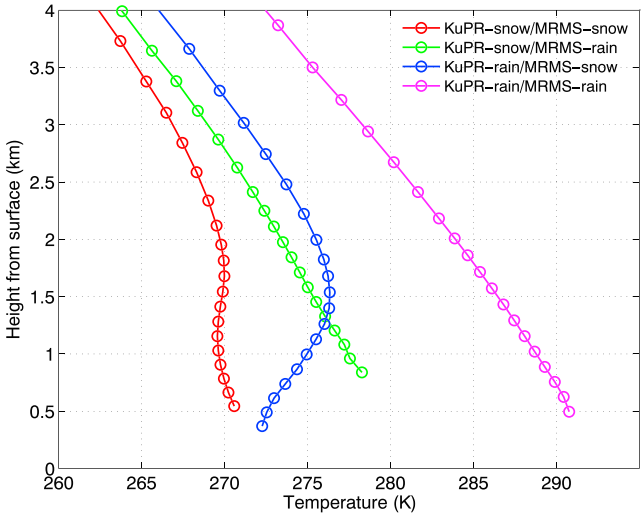

Figure 1. Temperature profiles under four different Ku-band precipitation radar (KuPR) and Multi-Radar/Multi-Sensor System (MRMS) precipitation phase scenarios.

Applications, version 2 (MERRA-2; Gelaro et al., 2017). These data sets have different spatial resolutions, and the following section discusses the collocation scheme.

3. Methodology

3.1. Downgrade the Higher-Resolution Observations

GPROF produces the near-surface precipitation rate at the resolution of the 18.7-GHz footprint size (~15 km). This is taken as the nominal resolution, and the finer spatial resolution GMI, KuPR, and MRMS observations are averaged (downgraded) to this coarser resolution.

Specifically, the native resolutions are ~7 km for 89 GHz, ~6 km for 166, 186, and 190 GHz, and ~5.2 km for KuPR at nadir. We average the nearest five ($(15/7)^2 \approx 5$) 89 GHz pixels, the nearest seven ($(15/6)^2 \approx 7$) 166, 186, and 190 GHz pixels, and the nearest nine ($(15/5.2)^2 \approx 9$) KuPR pixels to roughly match the area of GPROF foot print size (i.e., $15 \times 15 = 225$ km). A precipitating pixel is categorized as "snow (rain)" when all the precipitating pixels out of the nine selected KuPR pixels are flagged as "snow (rain)." Otherwise, the precipitation type is judged as "mixed," which are omitted from this study.

The 2-min MRMS observations at the spatial resolution of 0.01° are downgraded by locating the nearest MRMS observation to each GPROF pixel in time, then averaging all MRMS observations within the 15-km nominal resolution circle. When all the chosen MRMS precipitating pixels are flagged as "snow (rain)," the MRMS precipitation type is considered as "snow (rain)." This study omits "mixed" precipitation pixels. For both 2-m air temperature and temperature profile, we use the nearest grid to match the nominal resolution at the closest time.

3.2. Determine the Lag Time by Correlation Peak

Previous studies showed that the lag time values can differ depending on the statistical metrics. For example, Meng et al. (2017) showed a ~30-min lag time between snowfall rate derived from ATMS and MRMS based on correlation coefficient, while it is ~40 min based on the root-mean-square error (RMSE). Tan et al. (2018) found no consistent lag time value between four different metrics (Heidke skill score, bias, RMSE, and correlation). However, they did find that all metrics led to positive lag times, generally less than 20 min when comparing the rainfall rates from gauges with GPM KuPR, and the rainfall rates from gauges with GMI GPROF retrievals.

The present study uses correlations to investigate the lag time between TBs and surface precipitation rate. The correlations between TB at each frequency (V89...V190) and the surface precipitation rate are first computed at the simultaneous time. The times associated with the TB observations are increased by 2, 4, … , 120 min, then new correlation coefficients are computed between the surface precipitation rates and TB at each frequency. This produces 61 correlation coefficients, and this study defines the lag time as the time when the correlation peaks.

3.3. Precipitation Phase From MRMS and KuPR

This study uses the precipitation phase as defined by both MRMS and KuPR. The KuPR was incorporated to account for the portion of snowfall identified by MRMS that is likely to be mixed precipitation. The observations are grouped into four categories (with sample sizes indicated) to illustrate this point. The categories include (1) both KuPR and MRMS indicate rainfall (hereafter KuPR-rain/MRMS-rain, 987,920); (2) KuPR indicates rainfall, while MRMS indicates snowfall (hereafter KuPR-rain/MRMS-snow, 7,221); (3) KuPR indicates snowfall, while MRMS indicates rainfall (KuPR-snow/MRMS-rain, 71,780); and (4) both KuPR and MRMS indicate snowfall (KuPR-snow/MRMS-snow, 18,186). Figure 1 illustrates the mean temperature profiles from the surface to 4 km above ground level for these four scenarios.

Analyses show that only 71.58% (18,186/(7,221+18,186)) of the MRMS snowfall observations (corresponding to the blue and red temperature profiles in Figure 1) are judged as snowfall by KuPR at the near surface level (~1.5 km above the ground). This difference likely relates to the temperature inversion in the KuPR-rain/MRMS-snow category (corresponding to the blue temperature profile in Figure 1). The precip-

itation phase is more likely to be "frozen rain" rather than snowfall at the surface as indicated by MRMS. Alternatively, for MRMS indicated rainfall (corresponding to the green and purple temperature profiles Figure 1), the KuPR judges 93.39% as rainfall. The difference likely relates to the near surface temperature being colder than the surface temperatures (corresponding to the green temperature profile in Figure 1).

Although these analyses indicate the need for future work on phase determination by both MRMS and KuPR, that is not the purpose of the present study. The precipitation phase inconsistency between MRMS and KuPR is avoided herein by only using the observations when MRMS and KuPR agree on precipitation phase (i.e., only observations in KuPR-rain/MRMS-rain, and KuPR-snow/MRMS-snow categories).

4. Results

4.1. Delayed Correlation Between TB and Surface Precipitation Rate

This section analyzes the correlation between TB at different channels (V89, …, V190) and the surface precipitation rate at different time lags for both rain and snow. Similarities between H89/H166 and V89/V166 characteristics allow the following discussion to focus on results for V89, V166, V186, and V190.

For the rainfall scenario (Figure 2a), the correlation magnitude increases for all channels to correlation peaks at different time lags. The V89 (V186) correlation peaks ~8 min (~28 min) with the lag times from V166 and V190 in between. As previously introduced, the lag time differences among channels result from the different channels sensing hydrometeors at different altitudes. Previous work showed that the 89-GHz TB is more sensitive to hydrometeors near the surface, while the 186 GHz TB is more sensitive to hydrometeors near the storm top, under light and moderate precipitation scenarios (Seo & Liu, 2006; Skofronick-Jackson & Johnson, 2011). Figure 2a also reveals that the magnitude of the correlation increase differs for the different channels. For example, the strongest correlation between V89 and rainfall rate is at ~8 min, but not much improvement is shown relative to the simultaneous correlation. The magnitude of the correlation increase is greater for the other three channels, with V186 improving most from −0.24 to −0.30.

Grouping the rainfall data into storm top height categories reveals that the lag time difference decreases with increasing storm top height (not shown). There actually is no time lag difference between all channels for the category with storm top heights greater than 11.2 km (i.e., the 99th percentile of storm top height), which indicates that all channels (V89 to V190) are sensitive to the hydrometeors at similar altitudes. Previous radiative transfer model simulation experiments by Seo and Liu (2006) showed similar results. In these intense rainfall storms, the hydrometeors likely reach ground in less than 2 min.

Figure 2b clearly illustrates different patterns for the snowfall scenario relative to rainfall. First, the lag time is much longer for each channel. Specifically, the V89 and V186 lag times are ~20 and ~82 min in this category, compared with ~8 and ~28 min under the rainfall scenario. The much longer lag time is primarily caused by the slower falling speed of snowflakes relative to rain drops. Second, the magnitudes of the correlation increases are much larger for snowfall. For example, the correlation between V186 and the simultaneous snowfall rate is −0.12, while it increases to −0.30 at the 82-min lag time. Recall that under the rainfall scenario the V186 correlation only increases from −0.24 to −0.30.

4.2. Dependence on Environment Temperature and Storm Top Height for Snowfall

The environmental temperature and storm top height can affect the lag time in the snowfall scenario. The 10 temperature values nearest the surface (i.e., surface to ~1.5 km, Figure 1) are averaged to provide an indicator of the temperature influence on the time lag effect.

Figures 2c and 2d show the correlation between different channel TBs and surface snowfall rate at different time lags for average temperatures less than the 50th (270.6 K) and 25th (267.4 K) temperature percentiles. At temperatures below 270.6 K, the correlation variation features are similar to those shown for all data (Figure 2b). In contrast, the correlation magnitudes increase much more at the colder temperatures (<267.4 K, Figure 2d). For example, the V186 correlation increases from −0.02 for the simultaneous surface snowfall rate to −0.33 at the 46-min lag time.

The data are next subdivided into groups conditioned on the storm top height. For storm top greater than 3.9 km (50th percentile; Figure 2e) the correlation variation features are similar to those from all data (Figure 2b). However, for storm top heights greater than 4.6 km (75th percentile; Figure 2f) the lag times for all channels are much larger than those for all data (Figure 2b). The magnitude of the correlation increase is

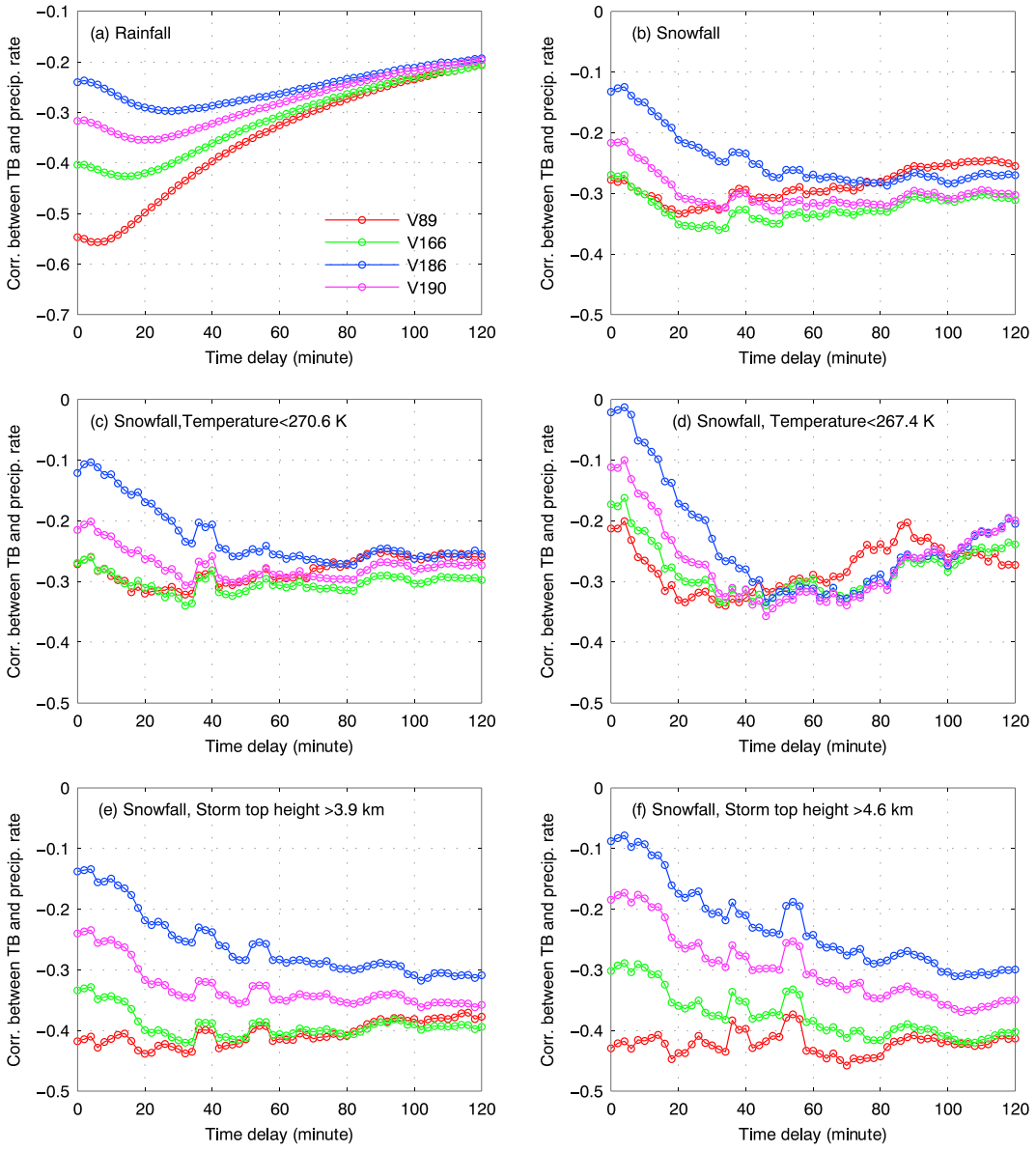

Figure 2. (a) The correlation between TB at different channels (V89, V166, V186, and V190) and the MRMS surface rain rate from the simultaneous time to 120-min time lag; (b) same as (a) except for snowfall; (c) same as (b) except the temperature is less than 270.6 K; (d) same as (b) except the temperature is less than 267.4 K; (e) same as (b) except the storm top height is larger than 3.9 km; and (f) same as (b) except the storm top height is larger than 4.6 km. The threshold values (270.6 K and 267.4 K) are the 50th and 25th percentiles of all temperature observations. The threshold values (3.9 and 4.6 km) are the 50th and 75th percentiles of all storm top height observations. TB = brightness temperature; MRMS = Multi-Radar/Multi-Sensor System.

much larger for V166, V186, and V190 for storm top heights greater than 4.6 km (cf. Figure 2f and Figure 2b). Similar analyses on rainfall observations revealed no clear dependence on different temperature or storm top height characteristics.

4.3. Impact for Precipitation Detection Evaluation

The time lag effect can lead to instances where the radiometer retrievals produce surface precipitation at the time of the satellite observation, while no simultaneous precipitation is indicated by the surface instruments. When evaluating the radiometer detection performance relative to the surface observations these pixels are classified as “false alarms.” Since these instances are caused by the different observation characteristics of

Table 1
The "False Alarm" Pixel Counts Relative to MRMS at the Simultaneous Time, and When Considering Three Time Lag Windows (i.e., 10, 30, and 60 min)

	0 min	10 min	30 min	60 min
Falsely detected pixel No.	1,425,917	1,218,186	1,085,421	988,057
Reduced by percentage	—	14.57%	23.88%	30.71%
False alarm ratio	34.56%	29.53%	26.31%	23.95%

Note. The false alarm ratio is also provided under each situation, which is defined as the falsely identified precipitating pixel number in GPROF-retrieval result divided by the total precipitating pixel number in GPROF-retrieval result. GPROF = Goddard Profiling Algorithm; MRMS = Multi-Radar/Multi-Sensor System.

different instruments, they should not be classified as "false alarms." These "false alarms" occurrences are next investigated by considering the time lag effect.

Data from the GMI GPROF retrievals and the MRMS ground radar observations are used to investigate this phenomenon. The GPROF retrievals are first classified as "false alarms" relative to the simultaneous MRMS observations, and then reclassified relative to the MRMS at times lags of 10, 30, and 60 min. The GPROF pixels classified as "false alarms" at the simultaneous time are reclassified as "correct" detections if MRMS observes precipitation within this time window. For the 10-min lag window, the GPROF retrievals are compared to five MRMS observations (i.e., 2, 4, 6, 8, and 10 min). If any of these five MRMS observations are associated with precipitation, this pixels is reclassified as a "correct" GMI detection.

Table 1 shows the results of this analysis. The 10-, 30-, and 60-min time lags reduce the "false-alarm" pixel count by 14.57%, 23.88%, and 30.71%, respectively. As expected, the false alarm ratio also decreases for longer time lag windows. Tan et al. (2018) noted a similar feature. Similar analysis is conducted by grouping data into snowfall and rainfall conditions. Although the numerical values differ under snowfall and rainfall, the degree of the false pixel number reduction and the false alarm ratio reduction is similar. This reduction of false alarms and false alarm ratio highlight the importance of considering the time lag effect in evaluating the level-2 retrieval results.

4.4. Impact for Precipitation Intensity Evaluation

The time-lag effect on the precipitation intensity is next evaluated when both GPROF and MRMS detect precipitation at the time of the satellite observation.

Figure 3a shows the correlation between GPROF-retrieved rain rate and MRMS rain rate. The correlation increases marginally up to a ~6-min lag time, and then decreases sharply for longer lag times. This indicates that the time lag effect is very weak under the rainfall scenario. Thus, the correlation between the simultaneous satellite-retrieved rainfall rate and surface rainfall rate is safe to use as a performance indicator.

The increasing correlation with increasing lag time is much more evident under snowfall conditions (Figure 3b). Most importantly, the correlation peaks at the ~20-min lag time (Figure 3b). The increasing correlation with increasing lag time is even more evident under cold temperature (Figure 3c) and for taller storms (Figure 3d). For example, for temperatures less than 267.2 K and storm top heights greater than 4.6 km, the lag time is ~30 min and the correlation increases from ~0.20 to ~0.46.

The larger correlation increase and time lag under snowfall condition implies that the weak correlation between the retrieved snowfall rate from radiometers and the surface-observed snowfall rate may not indicate poor snowfall retrieval performance (especially in cold environments and for tall storms). Thus, the time lag effect should be considered when evaluating the performance of the radiometer-derived snowfall retrievals in high latitudes.

It is important to note that GPROF uses multiple channels to retrieve the surface precipitation rate. The lag times based on TB at a certain channel (Figure 2) may differ from the lag times based on the precipitation rate retrievals (Figure 3). Regardless, analyses based on both TBs and precipitation rates retrieved from TBs show clear time lag effects relative to the surface observations.

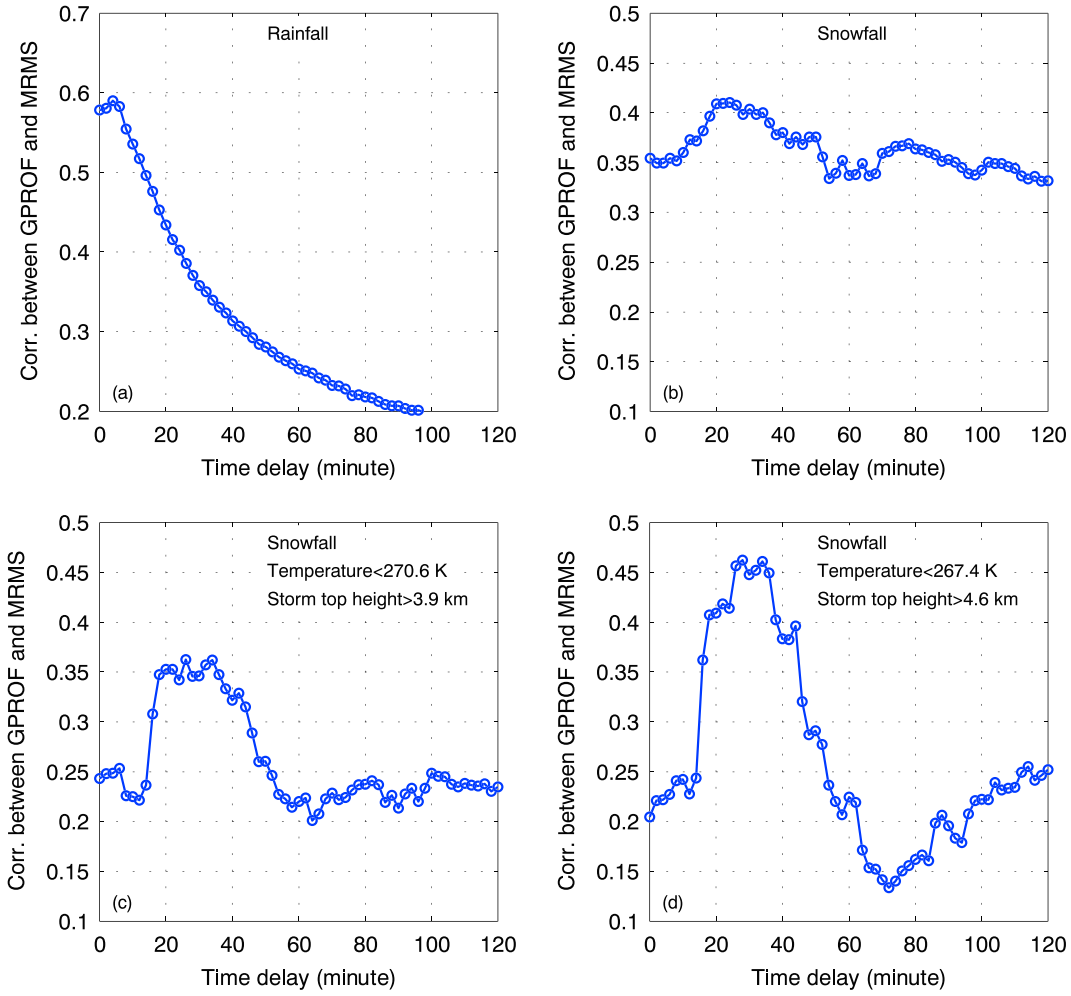

Figure 3. (a) The correlation between the GPROF-retrieved rainfall rate and the MRMS surface rainfall rate from the simultaneous time to 120-min time lag; (b) same as (a) except for snowfall; (c) same as (b) except the temperature is less than 270.6 K and the storm top height is greater than 3.9 km; (d) same as (b) except when the temperature is less than 267.4 K and storm top height greater than 4.6 km. The threshold values (270.6 K and 267.4 K) are the 50th and 25th percentiles of all temperature observations. The threshold values (3.9 and 4.6 km) are the 50th and 75th percentiles of all storm top height observations. GPROF = Goddard Profiling Algorithm; MRMS = Multi-Radar/Multi-Sensor System.

5. Conclusions and Discussions

This study investigates the correlation between TB and surface precipitation at different time lags using observations from GMI and the MRMS from 2014 to 2017 over CONUS. The GPROF-retrieved precipitation rate for GMI is also used to show the time lag effect on precipitation retrieval evaluations.

Delayed correlation is evident for both snowfall and rainfall situations, although the snowfall conditions resulted in larger magnitude correlation increases and longer lag times. This lag time and correlation magnitude increase was shown to depend on the environmental temperature and storm top height. The lag time and the correlation magnitude increase were larger for colder environments and taller storms. The influence of the time lag effect on precipitation detection and intensity evaluations also was examined. Results revealed that use of a 30-min lag time window can decrease "false alarms" by 23.88%. A very weak time lag effect was found for the rainfall intensity evaluation, with the largest correlation between the retrieved rain rate and the surface rain rate at (or very near) the simultaneous time. Alternatively, a clear lag time effect is observed under snowfall conditions. The correlation between the GMI-retrieved and MRMS snowfall rates peaked at a ~20-min lag time. The correlation magnitude increase and longer time lag were most evident in colder environments (<267.4 K) and for taller storms (>4.6 km).

This study shows that the lag effect must be considered when evaluating the radiometer detection performance relative to surface observations. As was shown, the hydrometeors may not reach the ground at the time of the satellite observation. These pixels should not be classified as "false alarms" since they directly relate to the different nature of the satellite and ground-based measurements. Caution should be exercised when using correlation as an indicator for evaluating the snowfall retrieval result from radiometers. The correlation can be very weak at the time of satellite observation, while the correlation can increase markedly when considering the lag time effect (especially in cold environments). This study implies that the radiometer-retrieved snowfall rates may need to shift forward (e.g., 30 min), especially in cold environments and for tall storms, before integrating the retrieval results into the level-3 merged products.

Acknowledgments
GPM data are downloaded from NASA Precipitation Processing System (PPS) website (https://storm.pps.eosdis.nasa.gov). MRMS precipitation data are downloaded from National Centers for Environmental Prediction (NCEP) (http://mrms.ncep.noaa.gov). MERR2 data are downloaded from NASA Goddard Earth Sciences (GES) Data and Information Services Center (DISC) (https://gmao.gsfc.nasa.gov). This work is supported by the NOAA grant NA14NES4320003 (Cooperative Institute for Climate and Satellites-CICS) at the Earth System Science Interdisciplinary Center, University of Maryland.

References

Amitai, E., Unkrich, C. L., Goodrich, D. C., Habib, E., & Thill, B. (2012). Assessing satellite-based rainfall estimates in semiarid watersheds using the USDA-ARS Walnut Gulch gauge network and TRMM PR. *Journal of Hydrometeorology*, *13*(5), 1579–1588.

Aonashi, K., Awaka, J., Hirose, M., Kozu, T., Kubota, T., Liu, G., et al. (2009). GSMaP passive microwave precipitation retrieval algorithm: Algorithm description and validation. *Journal of the Meteorological Society of Japan*, *87*(0), 119–136.

Bennartz, R., & Petty, G. W. (2001). The sensitivity of microwave remote sensing observations of precipitation to ice particle size distributions. *Journal of Applied Meteorology*, *40*(3), 345–364.

Boukabara, S.-A., Garrett, K., Chen, W., Iturbide-Sanchez, F., Grassotti, C., Kongoli, C., et al. (2011). MiRS: An all-weather 1DVAR satellite data assimilation and retrieval system. *IEEE Geoscience and Remote Sensing Magazine*, *49*(9), 3249–3272.

Dong, C., Yang, J., Zhang, W., Yang, Z., Lu, N., Shi, J., et al. (2009). An overview of a new Chinese weather satellite FY-3A. *Bulletin of the American Meteorological Society*, *90*(10), 1531–1544.

Draper, D. W., Newell, D., Wentz, F. J., Krimchansky, S., & Skofronick-Jackson, G. M. (2015). The Global Precipitation Measurement (GPM) Microwave Imager (GMI): Instrument overview and early on-orbit performance. *IEEE Journal of Selected Topics in Applied Earth Observation in Remote Sensing*, *8*, 3452–3462.

Ebtehaj, A. M., Bras, R. L., & Foufoula-Georgiou, E. (2015). Shrunken locally linear embedding for passive microwave retrieval of precipitation. *IEEE Transactions on Geoscience and Remote Sensing*, *53*(7), 3720–3736.

Edwards, P., & Pawlak, D. (2000). MetOp: The space segment for EUMETSAT's polar system. *ESA Bulletin*, *102*, 6–18.

Ferraro, R. R., & Marks, G. F. (1995). The development of SSM/I rain-rate retrieval algorithms using ground-based radar measurements. *Journal of Atmospheric and Oceanic Technology*, *12*(4), 755–770.

Foelsche, U., Kirchengast, G., Fuchsberger, J., Tan, J., & Petersen, W. A. (2017). Evaluation of GPM IMERG early, late, and final rainfall estimates using WegenerNet gauge data in southeastern Austria. *Hydrology and Earth System Sciences*, *21*(12), 6559–6572.

Foster, J. L., Skofronick-Jackson, G., Meng, H., Wang, J. R., Riggs, G., Kocin, P. J., et al. (2012). Passive microwave remote sensing of the historic February 2010 snowstorms in the Middle Atlantic region of the USA. *Hydrological Processes*, *26*(22), 3459–3471.

Gelaro, R., McCarty, W., Suárez, M. J., Todling, R., Molod, A., Takacs, L., et al. (2017). The modern-era retrospective analysis for research and applications, version 2 (MERRA-2). *Journal of Climate*, *30*(14), 5419–5454.

Goldberg, M. (2018). The joint polar satellite system overview. In *IGARSS 2018-2018 IEEE International Geoscience and Remote Sensing Symposium, IEEE* (pp. 1581–1584).

Gu, X., & Tong, X. (2015). Overview of China Earth observation satellite programs [Space Agencies]. *IEEE Geoscience and Remote Sensing Magazine*, *3*(3), 113–129.

Hou, A. Y., Kakar, R. K., Neeck, S., Azarbarzin, A. A., Kummerow, C. D., Kojima, M., et al. (2014). The global precipitation measurement mission. *Bulletin of the American Meteorological Society*, *95*(5), 701–722.

Huffman, G. J., Bolvin, D. T., Braithwaite, D., Hsu, K., Joyce, R., Xie, P., & Yoo, S.-H. (2015). NASA global precipitation measurement (GPM) integrated multi-satellite retrievals for GPM (IMERG). Algorithm Theoretical Basis Document Version2 4.

Kidd, C., Matsui, T., Chern, J., Mohr, K., Kummerow, C., & Randel, D. (2016). Global precipitation estimates from cross-track passive microwave observations using a physically based retrieval scheme. *Journal of Hydrometeorology*, *17*(1), 383–400.

Kulie, M. S., Bennartz, R., Greenwald, T. J., Chen, Y., & Weng, F. (2010). Uncertainties in microwave properties of frozen precipitation: Implications for remote sensing and data assimilation. *Journal of the Atmospheric Sciences*, *67*(11), 3471–3487.

Kummerow, C. D., Randel, D. L., Kulie, M., Wang, N.-Y., Ferraro, R., Joseph Munchak, S., & Petkovic, V. (2015). The evolution of the Goddard profiling algorithm to a fully parametric scheme. *Journal of Atmospheric and Oceanic Technology*, *32*(12), 2265–2280.

Li, R., & Min, Q. (2013). Dynamic response of microwave land surface properties to precipitation in Amazon rainforest. *Remote Sensing of Environment*, *133*, 183–192.

Liu, G. (2008). A database of microwave single-scattering properties for nonspherical ice particles. *Bulletin of the American Meteorological Society*, *89*(10), 1563–1570.

Meng, H., Dong, J., Ferraro, R., Yan, B., Zhao, L., Kongoli, C., et al. (2017). A 1DVAR-based snowfall rate retrieval algorithm for passive microwave radiometers. *Journal of Geophysical Research: Atmospheres*, *122*, 6520–6540. https://doi.org/10.1002/2016JD026325

Munchak, S. J., & Skofronick-Jackson, G. (2013). Evaluation of precipitation detection over various surfaces from passive microwave imagers and sounders. *Atmospheric Research*, *131*, 81–94.

Petersen, W., & Rutledge, S. (2001). Regional variability in tropical convection: Observations from TRMM. *Journal of Climate*, *14*(17), 3566–3586.

Petty, G. W., & Huang, W. (2010). Microwave backscatter and extinction by soft ice spheres and complex snow aggregates. *Journal of the Atmospheric Sciences*, *67*(3), 769–787.

Seo, E.-K., & Liu, G. (2006). Determination of 3D cloud ice water contents by combining multiple data sources from satellite, ground radar, and a numerical model. *Journal of Applied Meteorology*, *45*(11), 1494–1504.

Skofronick-Jackson, G., & Johnson, B. T. (2011). Surface and atmospheric contributions to passive microwave brightness temperatures for falling snow events. *Journal of Geophysical Research*, *116*, D02213. https://doi.org/10.1029/2010JD014438

Skofronick-Jackson, G., Petersen, W. A., Berg, W., Kidd, C., Stocker, E. F., Kirschbaum, D. B., et al. (2017). The global precipitation measurement (GPM) mission for science and society. *Bulletin of the American Meteorological Society*, *98*(8), 1679–1695.

Tan, J., Petersen, W. A., Kirchengast, G., Goodrich, D. C., & Wolff, D. B. (2018). Evaluation of global precipitation measurement rainfall estimates against three dense gauge networks. *Journal of Hydrometeorology*, *19*(3), 517–532.

Villarini, G., & Krajewski, W. F. (2007). Evaluation of the research version TMPA three-hourly 0.25× 0.25 rainfall estimates over Oklahoma. *Geophysical Research Letters*, *34*, L05402. https://doi.org/10.1029/2006GL029147

Wang, Y., Liu, G., Seo, E.-K., & Fu, Y. (2013). Liquid water in snowing clouds: Implications for satellite remote sensing of snowfall. *Atmospheric Research*, *131*, 60–72.

Wang, Y., You, Y., & Kulie, M. (2018). Global Virga precipitation distribution derived from three spaceborne radars and its contribution to the false radiometer precipitation detection. *Geophysical Research Letters*, *45*, 4446–4455. https://doi.org/10.1029/2018GL077891

Xie, P., Joyce, R., Wu, S., Yoo, S.-H., Yarosh, Y., Sun, F., & Lin, R. (2017). Reprocessed, bias-corrected CMORPH global high-resolution precipitation Estimates from 1998.

You, Y., & Liu, G. (2012). The relationship between surface rainrate and water paths and its implications to satellite rainrate retrieval. *Journal of Geophysical Research*, *117*, D13207. https://doi.org/10.1029/2012JD017662

You, Y., Wang, N.-Y., & Ferraro, R. (2015). A prototype precipitation retrieval algorithm over land using passive microwave observations stratified by surface condition and precipitation vertical structure. *Journal of Geophysical Research: Atmospheres*, *120*, 5295–5315. https://doi.org/10.1002/2014JD022534

You, Y., Wang, N.-Y., Ferraro, R., & Meyers, P. (2016). A prototype precipitation retrieval algorithm over land for ATMS. *Journal of Hydrometeorology*, *17*(5), 1601–1621.

You, Y., Wang, N.-Y., Ferraro, R., & Rudlosky, S. (2017). Quantifying the snowfall detection performance of the GPM microwave imager channels over land. *Journal of Hydrometeorology*, *18*(3), 729–751.

Zhang, J., Howard, K., Langston, C., Kaney, B., Qi, Y., Tang, L., et al. (2016). Multi-Radar Multi-Sensor (MRMS) quantitative precipitation estimation: Initial operating capabilities. *Bulletin of the American Meteorological Society*, *97*(4), 621–638.